Characterization of the Control Catabolite Protein of Gluconeogenic Genes Repressor by Fluorescence Cross-Correlation Spectroscopy and Other Biophysical Approaches

Silvia Zorrilla,*† Álvaro Ortega,* Denis Chaix,* Carlos Alfonso,‡ Germán Rivas,‡ Stéphane Aymerich,§ M. Pilar Lillo,† Nathalie Declerck,* and Catherine A. Royer*

*Institut National de la Santé et de la Recherche Médicale (UMR554), Centre de Biochimie Structurale, Centre National de la Recherche Scientifique (UMR5048), and Université Montpellier 1, F-34090 Montpellier, France; †Instituto de Química-Física "Rocasolano", Consejo Superior de Investigaciones Científicas, Serrano 119, E-28006 Madrid, Spain; ‡Centro de Investigaciones Biológicas, Consejo Superior de Investigaciones Científicas, Ramiro de Maeztu 9, E-28040 Madrid, Spain; and §AgroParisTech, Microbiologie et Génétique Moléculaire, F-78850 Thiverval-Grignon, France

ABSTRACT Determination of the physical parameters underlying protein-DNA interactions is crucial for understanding the regulation of gene expression. In particular, knowledge of the stoichiometry of the complexes is a prerequisite to determining their energetics and functional molecular mechanisms. However, the experimental determination of protein-DNA complex stoichiometries remains challenging. We used fluorescence cross-correlation spectroscopy (FCCS) to investigate the interactions of the control catabolite protein of gluconeogenic genes, a key metabolic regulator in Gram-positive bacteria, with two oligonucleotides derived from its target operator sequences, *gapB* and *pckA*. According to our FCCS experiments, the stoichiometry of binding is twofold larger for the *pckA* target than for *gapB*. Correcting the FCCS data for protein self-association indicated that control catabolite protein of gluconeogenic genes forms dimeric complexes on the *gapB* target and tetrameric complexes on the *pckA* target. Analytical ultracentrifugation coupled with fluorescence anisotropy and hydrodynamic modeling allowed unambiguous confirmation of this result. The use of multiple complementary techniques to characterize these complexes should be employed wherever possible. However, there are cases in which analytical ultracentrifugation is precluded, due to protein stability, solubility, or availability, or, more obviously, when the studies are carried out in live cells. If information concerning the self-association of the protein is available, FCCS can be used for the direct and simultaneous determination of the affinity, cooperativity, and stoichiometry of protein-DNA complexes in a concentration range and conditions relevant to the regulation of these interactions.

INTRODUCTION

Protein-DNA interactions play a central role in many biological processes, such as DNA replication, transcription, and repair. Thus, an in-depth investigation of the energetics and dynamics of the protein-DNA interactions involved and of the linked protein-protein and protein-ligand interactions is required to define the physical basis for these biological phenomena. Such quantitative information is essential for the mathematical modeling of gene regulation networks in systems biology. In particular, elucidation of the stoichiometries is crucial to the determination of the other parameters, such as the affinity and cooperativity, required to ultimately propose molecular mechanisms for regulation and control. Unfortunately, to date the experimental determination of protein-DNA complex stoichiometries has not proven straightforward, and reported affinities are frequently based on assumed stoichiometries.

Some insight into stoichiometry can be gleaned from gel mobility shift assays, although since this is not an equilibrium technique, the number and size of the complexes observed can depend upon the physical properties of the gel itself and the conditions of the electrophoreses. Moreover, absolute complex stoichiometries cannot be determined by this method. The highly reliable and quite powerful method of analytical ultracentrifugation (AUC) is often not ideal for protein-DNA complexes because these interactions can be of very high affinity and hence outside the concentration range required for AUC. Therefore, in AUC experiments carried out at these higher concentrations, different and higher order complexes are observed in many instances, and these are not relevant to the complexes formed under the equilibrium titration conditions. On the other hand, fluorescence anisotropy is sensitive enough to be used in the relevant nanomolar concentration range but is limited by the large size of the protein-DNA complexes compared with the relatively short lifetimes of the fluorescent dyes.

Moreover, the complexes are usually asymmetric and exhibit multiple rotational components (local dye motion, macromolecular flexibility) in addition to global complex tumbling, rendering rather difficult the interpretation of anisotropy data in terms of stoichiometry. The capacity of fluorescence cross-correlation spectroscopy (FCCS) methods for the determination of binding stoichiometries has recently been demonstrated. Kim et al. (1) determined the stoichiometry of the complexes of calmodulin and calmodulin-dependent protein kinase II in vitro and in live cells. In two other studies, the stoichiometry of the binding of labeled streptavidin and biotin as a model of ligand receptor interaction was investigated by

Submitted April 22, 2008, and accepted for publication July 17, 2008.

Address reprint requests to Catherine A. Royer, Centre de Biochimie Structurale, 29 rue de Navacelles, F-34090 Montpellier, France. Tel.: 33-4 67-41-79-02; Fax: 33-4-67-41-79-13; E-mail: catherine.royer@cbs.cnrs.fr.

Editor: David P. Millar.

0006-3495/08/11/4403/13 $2.00

doi: 10.1529/biophysj.108.135863

FCCS (2,3). This method has also been applied to assess the presence of more than one DNA duplex, within a single protein-DNA complex, by observation of the cross-correlation signal arising from oligonucleotides separately labeled with different fluorophores (4,5). However, we are not aware of studies reporting the use of FCCS-based titrations for the determination of the protein stoichiometry of protein-DNA complexes.

Single-molecule approaches such as FCCS constitute very powerful tools for the quantitative analysis of biomolecular interactions (6–8). In FCCS the fluctuations of the fluorescence in a confocal or two-photon excitation volume emitted by two diffusing macromolecules labeled with different dyes are separately detected in two channels to generate two autocorrelation curves and a cross-correlation function, which directly reflects the concentration of complex in the solution. Since its introduction by Schwille et al. (9), FCCS has been successfully applied for the quantitative analysis of biomolecular interactions in solution as well as in the cellular environment (6,7,10–13). The use of a two-photon laser as excitation beam, first proposed by Heinze et al. (14), constitutes a milestone in the development of FCCS methods (15). This is because it is important to use two dyes exhibiting emission at very different wavelengths to avoid channel cross talk (which is 100% cross correlated). Due to the relatively broad two-photon cross sections compared to one-photon absorption spectra, dyes exhibiting completely separable emission spectra can be simultaneously excited using two-photon laser as excitation beam. Therefore, there is no need to combine two visible lasers for achieving perfect overlap of the two detection volumes, which is usually challenging.

A number of scientific reports on the applications of FCCS for the thermodynamic analysis of protein-protein (2,12,16,17), protein-ligand (18,19), and protein-nucleic acid (4,5,20–23) interactions have appeared in the last decade. Like other fluorescence approaches, FCCS methods exhibit the requisite sensitivity for the study of very high affinity interactions. However, this sophisticated approach presents some advantages over hydrodynamic methods such as fluorescence anisotropy or single-channel fluorescence correlation spectroscopy (FCS), since there is no size limit to the complexes that can be detected. Moreover, the distance and the relative orientation of the dyes within the complex, critical for assays based on fluorescence resonance energy transfer, are irrelevant in FCCS-based determinations. Finally, the local rotational and lifetime properties of the dyes do not influence the signal.

In this study, we used FCCS, together with other fluorescence-based approaches and AUC, for characterizing the interaction of the control catabolite protein of gluconeogenic genes (CcpN) with two different DNA sequences. Recently completed genomic projects have led to the identification of a large number of new transcriptional regulatory proteins in prokaryotes, one of which is CcpN repressor, for which the molecular mechanisms of regulation remain to be determined. These studies have shown that, in the presence of glucose, CcpN downregulates the expression of two gluconeogenic genes, *gapB* encoding a nicotinamide adenine dinucleotide phosphate dependent glyceraldehyde-3-phosphate dehydrogenase, and *pckA* encoding a PEP-carboxykinase (24,25). A third gene, *sr1*, encoding a small untranslated RNA was also found to be repressed by CcpN under glycolytic conditions (26). The disruption of the *ccpN* gene severely affects the distribution of carbon fluxes through the main carbon metabolic pathways in *B. subtilis* (27). Moreover, CcpN homologs can be found in several firmicutes but not in Gram-negative bacteria (25), and there is a high level of homology between the CcpN cognate sequences in different Gram-positive bacteria. Therefore, investigation of CcpN mechanisms of repression may ultimately lead to the identification of target interactions for selectively controlling the growth of Gram-positive bacteria, some of which are pathogenic.

The target sequences of the CcpN regulator within the *pckA* and *gapB* operators have been investigated by footprinting experiments, and gel mobility shift assays were used to estimate the apparent affinities of the repressor for the operators (25,28). However, the exact DNA motifs recognized by CcpN are still not fully clarified, and at present there are two different proposals (25,28) (Fig. 1). In addition to the marked differences in the cognate sequences proposed in the two reports, in both cases, striking dissimilarities are found in the location and in the relative orientation or distance between the binding motives recognized by the repressor on the two target sequences. Any model for the repression of *gapB* and *pckA* operators by CcpN must explain how this regulator can recognize different target sequences. Moreover, the observed differences in the binding sequences seem to indicate that the actual mechanism of repression may be different for the two genes. In contrast, the first molecular studies on CcpN

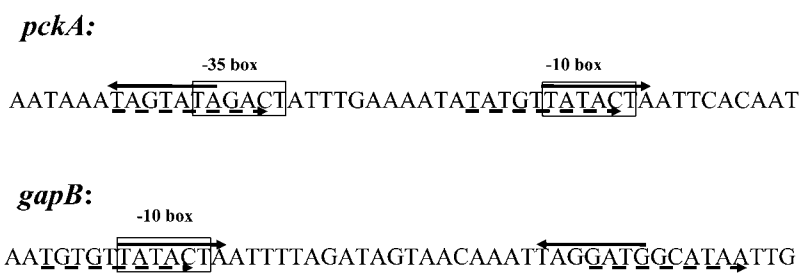

FIGURE 1 Sequences of the DNA oligonucleotides used in our study, the *gapB* and *pckA* targets. Solid and dashed arrows represent the binding sites proposed by Servant et al. (25) and Licht et al. (28), respectively.

interactions with its operators show very similar apparent affinity of binding to the *gapB* and *pckA* sequences (25,28). Interestingly, the stoichiometry of binding of the repressor to the operators, which may be key to understanding the molecular basis of the repression mechanism, has not yet been elucidated. Furthermore, although it has been suggested that CcpN repressor is able to form dimers, since it contains two protein interaction (cystathianon B synthase) domains in its C-terminus (25), the self-association behavior of the repressor in solution remains to be determined.

In this work we analyzed CcpN interactions with two oligonucleotides derived from the *gapB* and *pckA* operators using two-color two-photon FCCS. Using CcpN labeled with one dye, we conducted FCCS binding titrations of each of the two target oligonucleotides labeled with a second dye. We show that if one accounts for the self-association state of the free protein, then these titrations simultaneously provide information concerning not only the affinities but also the relative stoichiometries of the complexes. The stoichiometries deduced in this manner were confirmed by AUC experiments and hydrodynamic modeling. This study demonstrates clearly the power of FCCS for the quantitative analysis of the physical parameters governing protein-DNA interactions. Moreover, we address the strengths and limitations of FCCS methods for the determination of the absolute stoichiometries of protein-DNA complexes.

MATERIALS AND METHODS

Protein expression and purification

CcpN-His_6 cloned in the plasmid pPS2 was overexpressed in *Escherichia coli* Bl21(DE3) and purified by affinity chromatography, essentially as described in Servant et al. (25). After extensive dialysis versus 50 mM Tris-HCl, 300 mM NaCl, 2 mM EDTA buffer pH 8.0, aliquots of the purified protein were stored at −80°C. The protein concentration was determined by two independent methods, Bradford assay and ultraviolet (UV) absorbance, using a theoretically calculated molar extinction coefficient of 5200 $M^{-1}cm^{-1}$ at 280 nm. His-tagged CcpN has been shown to behave essentially as the wild-type repressor in vivo (D. Le Coq, unpublished results).

Fluorescent labeling of CcpN

CcpN was covalently labeled with fluorescein isothiocyanate, Alexa Fluor 488 carboxylic acid succinimidyl ester, and tetramethylrhodamine succinimidyl ester dyes (Molecular Probes, Invitrogen, Eugene, OR) on the amine groups directly after eluting from the Ni^{2+}-NTA agarose column during the purification protocol. Labeling with fluorescein isothiocyanate was performed by the addition of a 10-fold molar excess of the dye dissolved in dimethyl sulfoxide to a solution of CcpN in 0.1 M $NaHCO_3$, 150 mM NaCl, 2 mM Tris(2-carboxyethyl)phosphine, pH 8.0. The reaction was allowed to proceed at room temperature for 2 h with continuous agitation. For labeling with Alexa Fluor 488 carboxylic acid and tetramethylrhodamine succinimidyl ester dyes, the same protocol was followed but the pH of the reaction buffer was 8.3 and the molar excess of dye was fivefold. In all cases the reaction was stopped by adding 10% Tris-HCl 1 M, and the reaction mixture was loaded onto a PD 10 desalting column (GE Healthcare, Uppsala, Sweden) equilibrated in 50 mM Tris-HCl, 150 mM NaCl, and 2 mM EDTA pH 8.0 buffer. The ratio of labeling was estimated using the extinction coefficient of the dyes provided by the suppliers, 65,000, 71,000, and 68,000 $M^{-1}cm^{-1}$ for tetramethylrhodamine at 555 nm, Alexa 488 at 495 nm, and fluorescein at 494 nm, respectively, and that of CcpN in the UV (see above). The protein concentration was also measured by Bradford assay. In this way the degree of labeling was found to be 85%, 25%, and 20% for tetramethylrhodamine, Alexa 488, and fluorescein labeling, respectively.

DNA labeling

Unlabeled oligonucleotides containing the *pckA* and *gapB* target sequence of CcpN (Fig. 1), derivatized through phosphoramidite chemistry with an Amino-Link-2 (5′-aminohexylphosphate linker), which provides a primary amino group separated from the 5′ end by a six-carbon alkyl chain, were purchased from Sigma-Genosys (Heverhill, United Kingdom) in high performance liquid chromatography purified form. The oligonucleotide bearing the *pckA* target was labeled on the sense strand and that bearing the target on the antisense strand using Atto 647N succinimidyl ester (Atto-tec, Siegen, Germany) following the protocol described in Zorrilla et al. (29). Fluorescein-labeled sense and unlabeled antisense oligonucleotides containing the *pckA* and *gapB* target sequences, respectively, were purchased from the same company. The fluorescein labeling was performed by the supplier using phosphoramidite chemistry. The labeling ratios, estimated using the extinction coefficients of the DNA oligonucleotides at 260 nm and that of the Atto 647 N dye provided by the supplier (150,000 $M^{-1}cm^{-1}$ at 644 nm) were ~100%. The labeling ratio of the fluorescein-labeled oligonucleotides was estimated using an extinction coefficient of 80,000 $M^{-1}cm^{-1}$ at 490 nm. The sense and antisense strands were hybridized by heating a mixture containing a 10% excess of the nonlabeled strand to 90°C for 10 min and slowly cooling down to room temperature using a thermocycler.

Fluorescence cross-correlation spectroscopy

FCCS measurements were conducted using a setup based on a dual channel ISS Alba fluorescence correlation detector (ISS, Champaign IL) with avalanche photodiodes and a Zeiss Axiovert 200 microscope (Zeiss, Jena, Germany). The sample was excited by means of a Mai Tai HP femtosecond infrared (IR) tunable laser (Spectra-Physics, Newport, Mountain View, CA) tuned to 780 nm. The excitation light was focused into the sample by a Zeiss Apochromat 63× oil immersion objective (numerical aperture 1.4) through a 700 DCSXR dichroic mirror (Chroma Technology, Rockingham, VT) with an IR blocking filter, E700 SP 2P, HQ to eliminate the contribution of the IR excitation light in the detected signal. In the FCCS experiments performed on samples containing CcpN-Fl and Atto 647N-labeled DNA oligonucleotides, a 565 nm dichroic mirror was used to split the detected light onto two channels, and additional HQ675/50 nm and 525/50 nm band-pass filters were set before channels 1 and 2, respectively (Chroma Technology). The excitation power was set at 10 mW at the microscope entrance in all FCCS measurements. This power was determined to be a threshold one at which the autocorrelation traces became excitation power independent to avoid excitation saturation effects (30) as well as photobleaching.

The chambers used for the measurements were built by gluing a silicone insulator (Molecular Probes, Invitrogen) to a coverslip (Marienfeld, Lauda-Königshofen, Germany), and the samples were loaded into 10 μL wells. To prevent nonspecific absorption of the biological macromolecules to the surface of the coverslip, a pegylation treatment was carried out using Vectabond reagent and polyethylene glycol-succinimidyl ester as described elsewhere (31,32). Calibration of the detection volume was performed using a 70 nM fluorescein solution measured under identical illumination conditions as the samples. The beam waist ($w_0 \sim 0.35$–0.45 μm) and length ($z_0 \sim 0.7$–0.9 μm), recovered from analysis of the profiles observed for the fluorescein solution by fixing the 70 nM concentration of the dye and a translational diffusion coefficient of 300 $\mu m^2 s^{-1}$, were fixed parameters in the analysis of the auto- and cross-correlation curves recovered for the samples. FCCS measurements were performed by the addition of increasing concentrations of CcpN-Fl to 5 nM Atto 647N-labeled DNA oligonucleotides containing the target *pckA* and *gapB* oligonucleotides (Fig. 1). The

buffer was 50 mM Tris, 150 mM NaCl, 2 mM EDTA, 1% glycerol, 0.05 mg/mL bovine serum albumin, 2 mM dithiothreitol (DTT) pH 8.0. FCCS measurements were performed at sampling frequencies from 50 to 500 kHz, with identical results, and the time of measurement was 40 s for each trace. Each sample was measured 5–10 times, and the binding isotherms presented correspond to the average of at least four independent experiments.

Focusing a femtosecond pulsed infrared excitation laser beam through a high numerical aperture objective into a sample containing fluorescent species generates a tiny open volume element defined by two-photon excitation probability. In an FCCS experiment, molecules labeled with two spectrally different dyes are simultaneously excited, and the fluctuations in the fluorescence emission in this small volume are detected in two separate channels. In these experiments, three curves are generated by time correlation of the fluorescence intensity fluctuations detected, two autocorrelation functions arising from the green and red fluorophores $G_G(\tau)$ and $G_R(\tau)$ and one cross-correlation function, which accounts for the molecules in which the two fluorophores diffuse together $G_x(\tau)$. The autocorrelation and cross-correlation functions in the absence of cross talk can be written as follows:

$$G_i(\tau) = \frac{\langle \delta F(t)\delta F(t+\tau)\rangle}{\langle F(t)\rangle^2} \quad (1)$$

$$G_x(\tau) = \frac{\langle \delta F_G(t)\delta F_R(t+\tau)\rangle}{\langle F_G(t)\rangle\langle F_R(t)\rangle}, \quad (2)$$

where τ is the lag time. In the particular case of a system of freely diffusing species and assuming a three-dimensional (3D) Gaussian excitation profile, closed form expressions are derived from Eq. 1 and Eq. 2:

$$G_i(\tau) = G_i(0)\left(1+\frac{\tau}{\tau_{Di}}\right)^{-1}\left(1+\frac{\varpi_0^2\tau}{z_0^2\tau_{Di}}\right)^{-\frac{1}{2}} \quad (3)$$

$$G_x(\tau) = G_x(0)\left(1+\frac{\tau}{\tau_{Dx}}\right)^{-1}\left(1+\frac{\omega_0^2\tau}{z_0^2\tau_{Dx}}\right)^{-\frac{1}{2}}, \quad (4)$$

where $i = G$ or R and ω_o and z_o are the waist and length, respectively, of the three-dimensional Gaussian excitation volume at which the intensity drops to $1/e^2$. Here, τ_{Di} and τ_{Dx} are the translational diffusion time of species i and of the complex, respectively, and $G_i(0)$ and $G_x(0)$ are the amplitudes of the auto- and cross-correlation functions, respectively.

If no changes in the brightness of the fluorophores occur upon complexation, the amplitudes of the auto- and cross-correlation curves can be expressed as follows:

$$G_i(0) = \frac{\gamma}{V_{psf}C_{i,t}} \quad (5)$$

$$G_x(0) = \frac{\gamma C_x}{V_{psf}C_{G,t}C_{R,t}}, \quad (6)$$

where $i = G$ or R, $V_{PSF} = (\pi/2)^{3/2}\omega_0^2 z_0$, and $C_{i,t}$ and C_x are the total concentration of species i and of the complex, respectively. The γ-factor constitutes a measure of the uniformity of the fluorescence intensity observed for molecules at different positions within the detection volume and the effective steepness of the boundary defining the volume (30). For two-photon excitation and a 3D Gaussian profile, the value of γ is 0.125.

In an experiment in which the green species is titrated into a fixed concentration of the red one, the fraction of two-colored particles, f, may be calculated as follows (2,18):

$$f = \frac{C_x}{C_{R,t}} = \frac{G_x(0)}{G_G(0)}. \quad (7)$$

Analysis of the isotherm of binding generated by plotting the fraction of complex f versus the concentration of green species provides information on the binding affinity and cooperativity of the interaction. Moreover, under limiting conditions with a large excess of reactant G and fully bound R species, the relative cross-correlation amplitude tends to the brightness of the complex, η_x, relative to that of the green species, η_G, in the green channel (1):

$$\lim_{c\to\infty}\frac{G_e(0)}{G_G(0)} = \frac{\eta_x}{\eta_G}, \quad (8)$$

where $C = C_G/C_x$. Interestingly, if the *Green* species is always monomeric, then $\eta_x/\eta_G = n$, where n is the stoichiometry of the complex. In contrast, if the *Green* species (in our case the protein) itself tends to self-associate into higher order oligomers, then the ratio of amplitudes must be further corrected by the average self-association state of the protein, m (2 for dimer, 4 for tetramer, etc.), under conditions of a high excess of protein (*Green*) and fully bound *Red* species (oligonucleotide). This is because the particle number for the protein dimer is half that for a monomer, and hence the amplitude of the *Green* (protein) autocorrelation function must be divided by two for correct calculation of the stoichiometry. Note that, in any case, the ratio of amplitudes must also be corrected by the labeling ratio of the ligand r (1). Then, if there is no quenching, energy transfer or cross talk occur (as verified experimentally in the case here):

$$\left(\lim_{c\to\infty}\frac{G_x(0)}{G_G(0)}\right)\left(\frac{m}{r}\right) = n. \quad (9)$$

Analysis of the experimentally recovered auto- and cross-correlation curves was performed with the ISS Vista software, which uses a Marquardt-Levenberg minimization algorithm, assuming a 3D Gaussian point spread function. The goodness of the fits was judged by the recovered χ^2. There was no need to take into account triplet states in our data analysis. All the recovered autocorrelation and cross-correlation curves were best fit using a model involving two diffusing components. Autocorrelation traces were also fit using Globals software (Laboratory of Fluorescence Dynamics, Urbana, IL), and the errors in the output parameters were determined by rigorous confidence limit testing at 67%. The two programs, ISS Vista and Globals, yielded identical parameters for fits of the experimental traces.

The binding isotherms generated from the representation of the ratio of auto- and cross-correlation amplitudes versus CcpN concentration were analyzed using BIOEQS software (33). This software allows determination of the free energies of formation of the postulated complexes from the individual elements by using a numerical solver engine. BIOEQS uses a Marquardt-Levenberg algorithm to adjust all the parameter values to best fit the data. The error in the determined free energies is then estimated using the rigorous confidence limit testing at the 67% confidence level, in which the uncertainties arising from parameter correlations were taken into account.

Analytical ultracentrifugation

An Optima XL-A analytical ultracentrifuge (Beckman-Coulter, Palo Alto, CA) was used to perform the AUC experiments. The detection was carried out by means of an UV-visible absorbance detection system. Sedimentation equilibrium (SE) and velocity (SV) experiments were conducted using a Ti50 eight-whole rotor and standard (12-mm optical path) double sector centerpieces of Epon-charcoal. For samples containing fluorescein-labeled DNA, absorbance scans were taken at 495 nm, and the speed in the SV experiments was 40,000 rpm. The detection wavelengths were 550 and 230 nm for samples containing tetramethylrhodamine-labeled CcpN (TMR-CcpN) and nonlabeled CcpN, respectively. The SV experiments with these samples were carried out at a speed of 48,000 rpm. SE gradients were obtained using short columns (85 μl). For samples containing free Atto 647N-labeled oligonucleotides, the samples were centrifuged at two consecutive speeds: 13,500 and 17,000 rpm. SE experiments using samples of fluorescein-labeled DNA and nonlabeled CcpN were run using the overespeeding approach (34), with the aim of reducing the experimental timescale. The sample was first centrifuged at 30,000 rpm and then at 12,000 rpm to allow it to reach the equilibrium condition. In all SE experiments, a final centrifugation at high

speed (50,000 rpm) was performed to determine the baseline offset. The buffer in all SV and SE experiments was 50 mM Tris-HCl, 150 mM NaCl, 2 mM EDTA, 2 mM DTT, pH 8.0, and the temperature was 11°C.

Direct linear least squares boundary fitting of the experimental SV profiles was carried out using SEDFIT software to determine the sedimentation coefficient (S) distributions (35). All the s-values reported were corrected to standard conditions (20°C and water) using the software SEDNTERP (retrieved from the RASMB server (36)). The partial specific volume of CcpN and the buffer viscosity and density at different temperatures were also estimated by using SEDNTERP software. Whole-cell weight average buoyant molecular weights ($bMw = Mw(1 - \rho\nu)$, where Mw is the molecular weight, ρ is the density of the buffer, and ν is the partial specific volume of the solute) were obtained by fitting the equation describing the radial concentration distribution of an ideal solute at SE to the experimental data using the program EQASSOC (37). The SE gradients corresponding to samples containing mixtures of DNA and CcpN were analyzed using a model of mixtures of independently sedimenting solutes with the program MULTMX (kindly provided by Dr. Allen Minton, National Institutes of Health). Determination of the molecular weight of the macromolecular mixtures from the output buoyant masses is not straightforward, since the partial specific volumes of protein (0.74 mL/g) and DNA (0.55 mL/g) are very different. Therefore the SE data of the macromolecular mixtures were analyzed assuming the linear approximation for the buoyant masses:

$$bM_{w,ij} = ibM_{w,A} + jbM_{w,B}, \tag{10}$$

where ij refers to the complex A_iB_j, and $bM_{w,A}$ and $bM_{w,B}$ are the buoyant molecular weights of pure A and pure B, respectively (38).

Hydrodynamic modeling

The modeling of the structures for the properties calculation was made using ellipsoids from the crystallographic structures of the regulatory domain (RD-CcpN) and the DNA binding domain of the CcpN protein and a cylinder for the DNA fragment. From the atomic coordinates of RD-CcpN and the HTH, we calculated the hydrodynamic properties using the program HYDROPRO (39). The HTH atomic coordinates were obtained from a known helix-turn-helix (HTH) crystallographic structure (from the Diphtheria Tox Repressor, Protein Data Bank code: 1F5T) and manipulated to have the length of the fragment corresponding to the noncrystallized part in the RD-CcpN structure. Using the program HYDFIT (40), we obtained the dimensions of the ellipsoids that fit these properties. The model for the DNA fragment was just a cylinder with the typical dimensions of the DNA double helix: 3.4 Å length per basepair (bp) and 24.5 Å diameter. Finally, we built the models for the different complexes with those subunits; and using the program HYDROSUB (41), we calculated the hydrodynamic properties of the different conformations and stoichiometries, including the sedimentation coefficient and the translational diffusion coefficient.

Steady-state fluorescence anisotropy

Steady-state fluorescence anisotropy binding titrations were carried out using a PC1 photon counting steady-state ISS (Champaign, IL) spectrofluorometer regulated at 20°C using quartz cuvettes (Starna, Hinault, UK) of 3 × 3 mm path length. Ten measurements were taken per sample, each of them during 50 s. Anisotropy values plotted represent the average of 5–7 values measured by the instrument after equilibration. The curve reported is the average of four independent experiments. The excitation and emission wavelengths were 495 and 520 nm, respectively. The buffer for the measurements was 50 mM Tris-HCl, 150 mM NaCl, 1% glycerol, 0.05 mg/mL bovine serum albumin, 2 mM EDTA, 2 mM DTT, pH 8.0. Analysis of the experimental binding curves was conducted using BIOEQS software (see above).

Time-resolved fluorescence

Picosecond-resolved fluorescence intensity and anisotropy measurements were carried out using a Spectra Physics (Mountain View, CA) titanium:sapphire mode-locked laser, associated to a second harmonic generator tuned at 460 nm (as described in Lillo et al, 2002). The time resolution was 12.2 ps/channel. The intensity decays were analyzed to a triexponential function of the form

$$I_m(t) = \sum_i a_i \exp(-t/\tau_i), \tag{11}$$

where $I_m(t)$, τ_i, and a_i are the fluorescence intensity decay at magic angle (54.7°), the fluorescence lifetimes and the preexponential factors, respectively $\left(\sum a_i = 1\right)$. The fluorescence anisotropy decay was determined by simultaneous analysis of the parallel and perpendicular emission intensity components. The anisotropy fitting function was a sum of exponentials of the form (42)

$$r(t) = r(0) \sum_i \beta_i \exp(-t/\varphi_i), \tag{12}$$

where $r(0)$ is the time-zero anisotropy, φ_i the rotational correlation times, and β_i the fractional amplitudes. Data analysis was performed by nonlinear least squares global fit using Globals software (Laboratory of Fluorescence Dynamics). The quality of the fit was determined from global χ^2 values and visual inspection of the weighted residuals distribution. The errors were estimated by rigorous confidence limit testing at the 67% confidence level using the same software.

RESULTS

CcpN binds to *gapB* and *pckA* targets with different stoichiometry

We conducted two-color, two-photon fluorescence cross-correlation spectroscopy based titrations of DNA oligonucleotides derived from the *pckA* or *gapB* operators of CcpN (Fig. 1). These titrations were performed by the addition of fluorescein-labeled CcpN (CcpN-Fl) into solutions containing a fixed (5 nM) concentration of the DNA oligonucleotides, which were covalently modified with the fluorescent dye Atto 647N. The two fluorophores, fluorescein and Atto 647N, were selected on the basis of their well-separated fluorescence emission spectra, which eliminate artifactual cross correlation arising from channel cross talk. Nevertheless, before starting the titrations, suitable controls were performed to verify the lack of cross talk as well as to determine the experimental dynamic range and to select the appropriate conditions to investigate the specific binding of the protein to the target DNAs. To this end, we recorded the auto- and cross-correlation signals arising from samples containing CcpN-Fl and an Atto 647N-labeled nonspecific DNA oligonucleotide of approximately the same length (45 bp) as those containing the *gapB* and *pckA* sequence.

The addition of up to 1.3 μM CcpN, 250 nM of which actually bore the fluorescein dye, to 5 nM nonspecific labeled DNA resulted in a negligible cross-correlation signal (results not shown). Therefore, below 1.3 μM CcpN, the signal of the Atto 647N-labeled DNA is detected only in the red channel and the signal of the fluorescein-labeled protein is detected only in the green channel; hence any cross-correlation signal arises only from actual physical interaction of the repressor with the operator. Moreover, the lack of cross correlation when using this nonspecific oligonucleotide rules out a contribution of nonspecific electrostatic protein-DNA inter-

actions under the conditions of the assay, that is, 150 mM NaCl concentration and pH 8.0. This observation was further confirmed by steady-state fluorescence anisotropy titrations of the same nonspecific DNA oligonucleotide, in this case labeled with Cy3B (results not shown). No interaction with the repressor was detected at 150 mM NaCl, although at 50 mM NaCl the anisotropy of the labeled DNA notably increases upon addition of CcpN. Thus, the investigation of the specific binding of CcpN repressor to the operators was always carried out in solutions containing 150 mM NaCl, and in the FCCS binding titrations the CcpN concentration was kept below 1.3 μM to avoid cross talk between the channels.

Representative examples of auto- and cross-correlation curves recovered in the course of the titrations of the *gapB* and *pckA* operators with CcpN repressor are shown in Fig. 2. Emission from the fluorescein-labeled CcpN was detected in the green channel. Because of the low concentration of DNA in the solutions (5 nM), most of the signal recorded in the green channel corresponds to free CcpN-Fl, in particular at high concentrations of the repressor. The red channel (Fig. 2, *insets*) exhibits a 10-fold higher autocorrelation amplitude due to the low concentration of target oligonucleotide labeled with the red dye. It is noteworthy that no quenching of the fluorescein dye attached to CcpN or the Atto 647N fluorophore born by the DNA oligonucleotides was observed upon interaction. Moreover, no change in intensity was observed for the CcpN-Fl upon interaction with unlabeled specific DNA. Hence the intrinsic molecular brightness of the dyes was not affected by complexation.

The amplitude of the autocorrelation functions at time zero from the green, $G_G(0)$, and red, $G_R(0)$, channels yield the total concentration of fluorescein-labeled repressor and Atto 647N-labeled operator, respectively. Moreover, the time-zero amplitude of the cross-correlation function, $G_x(0)$, allows calculation of the amount of complex in the solution. We note that the cross-correlation amplitudes in Fig. 2 are relatively low because of the low fluorescence labeling ratio of the protein (20%). A significant change in the amplitude of cross correlation was observed upon addition of CcpN, indicative of binding. Hence, a plot of the ratio of the amplitudes of the cross correlation between the protein and DNA channel and the autocorrelation from the protein channel, $G_x(0)/G_G(0)$, versus the total concentration of repressor corresponds to a binding isotherm (Fig. 3) (2).

Before analysis of the binding curves, we used the asymptotic value of the $G_x(0)/G_G(0)$ ratio to calculate the stoichiometry for the CcpN complexes with the two target oligonucleotides (see Materials and Methods and Kim et al. (1)). We first corrected the $G_x(0)/G_G(0)$ ratio by the labeling ratio of the repressor (20%) (1). In addition, unlike previously published studies in which the free ligand was always monomeric (1–3), in the case here, one must also correct by a factor that reflects the self-association state (and hence the lower particle number with respect to monomer) of the protein. We determined by using other techniques (see below) that in the high nanomolar concentration range, where the plateau of the curves is reached, CcpN predominantly forms dimers. Hence the $G_x(0)/G_G(0)$ ratio at the plateau must be multiplied by this factor of two, yielding an apparent stoichiometry for the CcpN/oligonucleotide complexes of 1.6 for the *gapB* target and 3.0 for the *pckA* target. Clearly, the stoichiometry observed for the *pckA* target is twofold higher than that observed for the *gapB* target. Moreover, since fractional stoichiometries are not physically possible, at this point we postulate a dimeric CcpN/*gapB* complex and a tetrameric CcpN/*pckA* complex.

Further information concerning the stoichiometry of the complex can be deduced from analysis of the time dependence of the correlation profiles. All the profiles recovered (auto and cross) were best fit to a model involving two diffusing species (Table 1). The faster translational diffusion coefficient 68 $\pm$ 6 $\mu m^2/s$, retrieved from global analysis of the autocorrelation traces observed in the green channel at the plateau reflects, as noted above, essentially free CcpN, given the very low concentration of DNA. Its value was intermediate between that predicted for dimeric (59 $\mu m^2/s$) and monomeric (77 $\mu m^2/s$) CcpN (41), although the precision of FCS analyses precludes resolution of dimerization phenomena. As expected, the translational diffusion coefficients retrieved from analysis of the cross-correlation curves were

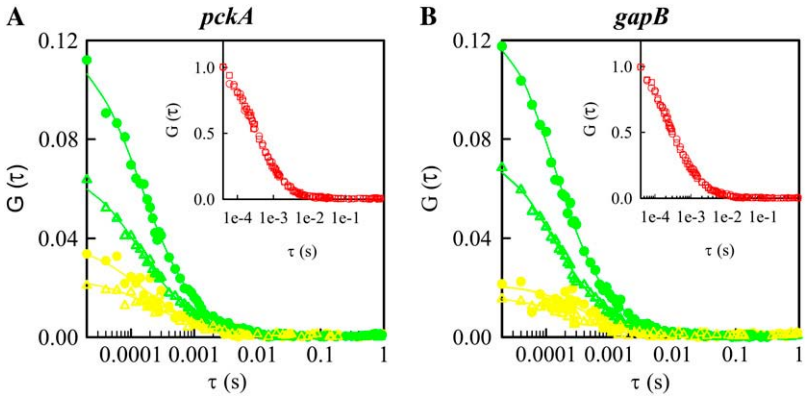

FIGURE 2 Representative examples of the auto- and cross-correlation profiles recovered from FCCS measurements of the interaction of fluorescein-labeled CcpN with the Atto 647N-labeled oligonucleotides bearing the *pckA* (*A*) and *gapB* (*B*) target sequences. Green, red, and yellow curves correspond to the autocorrelation traces recorded in the green and red channels and the cross-correlation curve, respectively. The total concentration of CcpN was either 468 nM (*closed circles*) or 800 nM (*open triangles*). The concentration of DNA was 5 nM. In the insets, the autocorrelation traces recorded in the red channel at 0 (*open circles*) and 1.3 (*open squares*) μM repressor are plotted. Solid lines correspond to best fits of the curves to the models discussed in the main text.

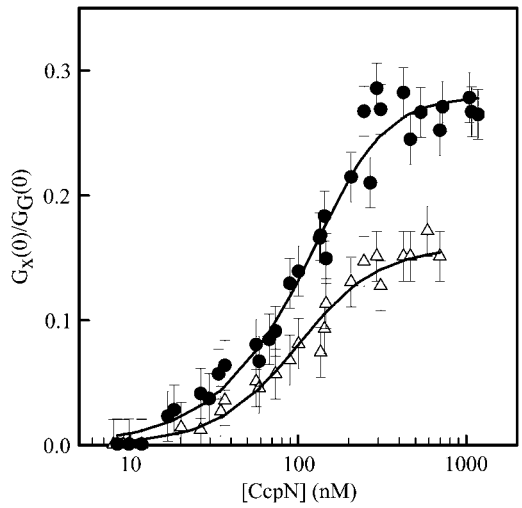

FIGURE 3 FCCS-based titrations of the Atto 647N-labeled *gapB* (*triangles*) and *pckA* (*circles*) target oligonucleotides, with the fluorescein-labeled repressor. $G_x(0)$ and $G_G(0)$ are the amplitudes of the cross correlation and protein autocorrelation functions retrieved from the fitting of the profiles. The ratio $G_x(0)/G_G(0)$ represents the fraction of complex with respect to the total concentration of DNA, and the high concentration plateau of the curves is proportional to the stoichiometry of the complexes (see the main text). Solid lines correspond to the best fits of the data to the energetic models discussed in the main text. The concentration of DNA in the titrations was 5 nM.

slower than those observed in the green and red channels (Table 1), since cross correlation arises only from the protein/DNA complexes and not from the free species. A fraction, never exceeding 15%, of slow diffusing species ($D < 10$ $\mu m^2/s$) was required to fit all the auto- and cross-correlation profiles, probably indicating the presence of irreversible macromolecular aggregates.

The apparent stoichiometries recovered above are lower than expected. That for the *gapB* target, 1.6, is unphysical, since stoichiometries are necessarily whole numbers. Hence, the calculated values must reflect additional contributions. The FCS curves corresponding to the protein always exhibit a fraction (5%–15%) of irreversible aggregates with translational diffusion coefficients between 1 and 5 $\mu m^2/s$. It is important to remark that despite their low proportion, since they involve a large number of molecules, their contribution to the amplitude of the autocorrelation profile is significant. Indeed, the $G_G(0)$ value for the protein is higher than it would be in the absence of these aggregates. This leads to an underestimation of the complex stoichiometry. If we correct the amplitude ratios assuming a 10% contribution from a 12-mer ($D = 4.8$ $\mu m^2/s$), we calculate a stoichiometry of 2 for the *gapB* target and 4 for the *pckA* target.

TABLE 1 Translational diffusion parameters retrieved from analysis of FCCS curves

	D_1 *pckA*	D_1 *gapB*
Red channel	61 (−6, +9)	61 (−5, +11)
Green channel	66 (−5, +6)	69 (−4, +6)
Cross correlation	41 (−11, +20)	44 (−9, +21)

Data presented correspond to the best fit of the profiles to a two diffusing species model. D_1 is the translational diffusion coefficient of the fast diffusing species in $\mu m^2/s$, whose contribution to the red autocorrelation, green autocorrelation, and cross-correlation functions is >85%, >90%, and >95%, respectively. Errors were calculated by rigorous confidence limit testing at the 67% confidence level.

Self-association of CcpN

Clearly the determination of the self-association state of the repressor at the binding plateau is crucial for the determination of absolute stoichiometry values by FCCS. To this end, a combined approach including different biophysical techniques was used to investigate the solutions containing free repressor protein. First, SV experiments were conducted on samples containing TMR-CcpN at different concentrations. It is noteworthy that labeled protein was used in this experiment to access low concentrations of protein, relevant to the DNA titrations, by taking advantage of the more than 10-fold larger molar extinction coefficient of the dye in the visible compared with that of the protein in the UV. Analysis of SV results from solutions containing 1.3 μM TMR-CcpN yielded sedimentation coefficient distributions displaying a single peak at 3.4 S (Fig. 4 *A*), in good agreement with the sedimentation coefficient of 3.0 S estimated by hydrodynamic modeling for dimeric CcpN. Increasing the concentration of CcpN in the solutions resulted in more heterogeneous sedimentation coefficient distributions exhibiting an additional peak around 6 S, indicative of higher order protein associations at higher concentrations.

Since the interaction of CcpN repressor with the operators occurs between 10 nM and 1 μM, we wanted to explore its self-association in this range. Therefore, we turned to highly sensitive fluorescence spectroscopy methods such as steady-state and time-resolved fluorescence anisotropy. Steady-state fluorescence anisotropy of CcpN-Alexa 488 solutions was monitored as a function of the total protein concentration (Fig. 4 *C*). Although the anisotropy change was rather small, a significant protein concentration dependence was observed, which can be interpreted in terms of monomer-dimer equilibrium. The free energy change retrieved from analysis of the binding isotherm was -9.1 ± 0.3 kcal/mol ($K_d = 170$ nM). It is noteworthy that the total intensity recovered from the solutions scaled linearly with protein concentration, thus ruling out any contribution of changes in the fluorescence emission properties of the dye to the anisotropy decrease detected.

Furthermore, time-resolved fluorescence measurements were carried out on samples containing Alexa 488-labeled CcpN at 1 μM, 700 nM, 500 nM, and 300 nM total protein concentration. The intensity decays recovered for all these samples were best fit to a triple exponential decay model, with lifetimes of 4.1 (70%), 2.3 (16%), and 0.4 (14%) ns.

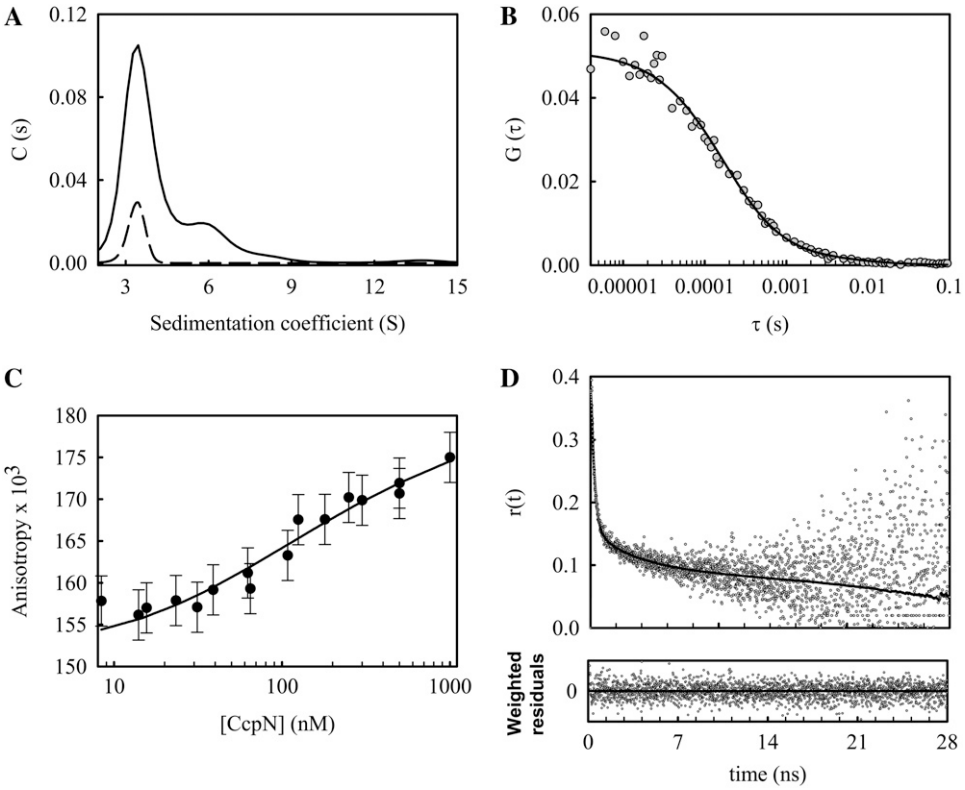

FIGURE 4 Hydrodynamics of the free CcpN repressor in solution. (*A*) Sedimentation coefficient distributions determined for 1.3 μM TMR-CcpN (*solid line*) and for 30 μM nonlabeled CcpN (*dashed line*). The distributions shown have been corrected to standard conditions (20°C). (*B*) Low resolution hydrodynamic model built for CcpN dimer. The theoretical sedimentation coefficient of the modeled molecule is indicated. (*C*) Steady-state fluorescence anisotropy of Alexa 488-labeled CcpN as a function of protein concentration. The solid line in the graph corresponds to the fit of the binding isotherm to a monomer-dimer model. $\lambda_{exc} = 495$ and $\lambda_{em} = 520$. (*D*) Fluorescence anisotropy decay determined for Alexa 488-labeled CcpN at 1 μM total protein concentration. The fit shown corresponds to a triexponentional model (see the main text). $\lambda_{exc} = 460$ and $\lambda_{em} = 520$.

These measurements confirm the lack of changes in the lifetimes of the fluorophore with protein concentration. Time-resolved fluorescence anisotropy decays of the Alexa 488-labeled CcpN were simultaneously fit to a triexponential rotational model (Table 2). In the fits, the time-zero anisotropy was fixed to 0.38 (43). The two fast rotational correlation times determined can be assigned to local motions of the dye (0.2 ns) and some kind of internal flexibility within the protein (~2 ns). The preponderant contribution of these two depolarization components (>65%) explains why such modest steady-state anisotropy change was detected upon dissociation of the dimer.

The third rotational correlation time retrieved from analysis of the decays corresponds to the global tumbling of the macromolecule, which according to our low resolution models would be 55 ns for dimeric CcpN. This time is very long compared with the fluorescence lifetime of the Alexa 488 dye, and hence it is not well resolved in our analysis. However, decreasing the protein concentration shortens the correlation time to a value close to that expected for a CcpN monomer. The value also becomes better resolved. The combination of these biophysical approaches strongly supports 1), the existence of a monomer-dimer equilibrium for CcpN in the concentration range in which the interaction with the operators occurs; and 2), the fact that in the plateau region of the FCCS experiments, CcpN predominantly populates a dimer.

TABLE 2 Rotational diffusion parameters of CcpN-Alexa 488

[CcpN] (nM)	ϕ_2 (ns) ± 0.3	ϕ_3 (ns)
1000	1.9	37 (−17, + 47)
700	1.9	33 (−15, +54)
500	1.8	28 (−12, +70)
300	1.3	24 (−4, +11)

ϕ_i and β_i are the rotational correlation times and their amplitudes, respectively, with $\sum\beta_i = 1$. Here ϕ_1, β_1, and β_2 were 0.23 ± 0.02 ns, 0.55 ± 0.03, and 0.13 ± 0.05, respectively. r_0 was fixed to 0.38 (43). In the fits, χ^2 recovered was always below 1.3, and the errors were calculated by rigorous confidence limit testing at the 67% confidence level. $\lambda_{exc} = 460$ $\lambda_{em} = 520$.

CcpN binds to *pckA* and *gapB* oligonucleotides as a tetramer and a dimer, respectively

Given the biochemical issues (labeling ratio and irreversible aggregation) that necessitate correction of the FCCS results, we wanted further confirmation of the absolute stoichiometry using an independent method, AUC by combination of its two major approaches, SE and SV. Thus, we conducted both SE and SV experiments on samples containing fluorescently labeled DNA *pckA* and *gapB* target oligonucleotides in the absence and presence of different amounts of the repressor protein.

Sedimentation velocity

Analysis of SV experiments performed on solutions containing the fluorescein (2.8 μM) or Atto 647N (1.5 μM) labeled oligonucleotides in the absence of CcpN in terms of a distribution of sedimentation coefficients yielded a single peak at 3.3–3.5 S (Fig. 5), in good agreement with that (3.2 S) calculated for an

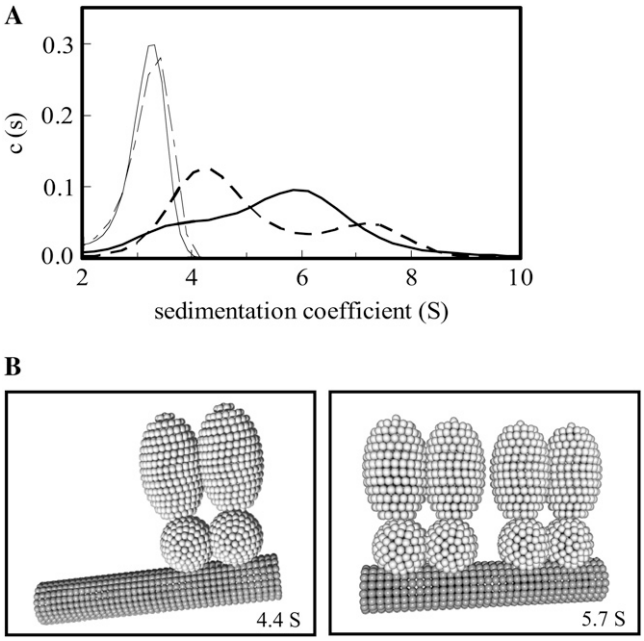

FIGURE 5 Sedimentation coefficient distributions recovered for the complexes of the CcpN repressor with the target *gapB* and *pckA* oligonucleotides. (*A*) 2.8 μM fluorescein-labeled *gapB* (*dashed*) or *pckA* (*solid*) oligonucleotides in the absence (*thin lines*) and presence (*thick lines*) of a sevenfold molar excess of nonlabeled repressor. The distributions shown have been corrected for standard conditions (20°C). (*B*) Low resolution models of dimeric and tetrameric CcpN in complex with a 49 bp DNA oligonucleotide. The calculated sedimentation coefficients of the modeled complexes are indicated.

appropriate DNA model (41). SE experiments also were best fit to a model involving a single species (Fig. 6, *A* and *B*). The molecular weights obtained accounting for buoyant molar masses are compatible with the 30,700 Da molecular mass of the DNA oligonucleotides. Therefore, the target DNAs used in this study were present as homogeneous species.

SV experiments carried out on solutions of the labeled oligonucleotides in the presence of an excess of nonlabeled CcpN repressor yielded different sedimentation coefficient distributions for complexes with the *gapB* or *pckA* targets. In the presence of a sevenfold molar excess of CcpN (in monomer units) with a 2.8 μM solution of the fluorescein-labeled *gapB*, target distributions involving two peaks were observed: a major peak at ~4.3 S and another centered around 7.2 S (Fig. 5 *A*). In the case of the *pckA* target, sedimentation coefficient distributions involving two main peaks were also observed, with a major peak centered at 5.9 S and a minor one at ~3.8 S. These experiments clearly show a different hydrodynamic behavior of CcpN complexes depending on the target sequence involved.

Hydrodynamic modeling of CcpN complexes

To interpret the peaks recovered in the sedimentation coefficient distributions in terms of protein/DNA complex stoichiometries, low resolution models were built for postulated complexes of different stoichiometries, whose hydrodynamic properties were afterward theoretically calculated and compared with the experimentally determined ones. Note that since the protein is not labeled, species containing exclusively free protein are not detected in the SV experiments conducted. The models were built from the crystallographic structures of the RD-CcpN, which was recently obtained (S. Arold, S. Aymerich, D. Chaix, N. Declerck, K. De Guillen, D. Le Coq, and C. Roumestand, unpublished results), and the DNA binding domain. We employed HYDFIT (40) to build the ellipsoidal models of the subunits and then HYDROSUB (41) to calculate the hydrodynamic properties of the structures.

A sedimentation coefficient of 4.4 S resulted from the calculation of the hydrodynamic properties of a complex involving 2 CcpN monomers and a single molecule of a 49 bp DNA oligonucleotide, arranged as shown in Fig. 5, and in good agreement with the major peak (4.3 S) found for the CcpN/*gapB* complex. The major peak observed in the *pckA*/CcpN solutions at 5.8 S is compatible with the sedimentation coefficient of 5.7 S, theoretically predicted for a complex in which 4 CcpN monomers bind to one molecule of the *pckA* target, generating the complex shown in Fig. 5.

Sedimentation equilibrium

To further validate the stoichiometry of the complexes of CcpN repressor with the two target oligonucleotides, SE experiments were undertaken. The design of the equilibrium experiments for solutions of this regulatory protein was not straightforward, since CcpN did not retain its binding activity during the long time required to attain the equilibrium condition (more than 1 day). This limitation was overcome by application of the overspeeding approach (see Materials and Methods), which allowed reducing considerably the experimental timescale (34). As in the SV experiments shown above (Fig. 5), SE measurements were carried out with samples containing 2.8 nM of the fluorescein-labeled *pckA or gapB* oligonucleotides and sevenfold molar excess of CcpN, in monomer units. Since SV analysis clearly demonstrates the heterogeneity of the CcpN/DNA solutions used in the AUC assays, the experimentally determined SE gradients were analyzed using two-species models (Fig. 6).

In the analysis, the buoyant molar masses were fixed to those of the expected species, according to the interpretation of the sedimentation coefficient distributions observed for each solution in light of our molecular models. Thus, in the analysis of the output gradient associated with the CcpN/*pckA* sample, buoyant molar masses of 13,699 and 39,619 (calculated from the molecular mass of the DNA and the protein and their partial specific volumes; Materials and Methods), corresponding to free DNA and to a complex involving 4 CcpN monomers and 1 DNA molecule, respectively, were fixed parameters. Best fits of this gradient were

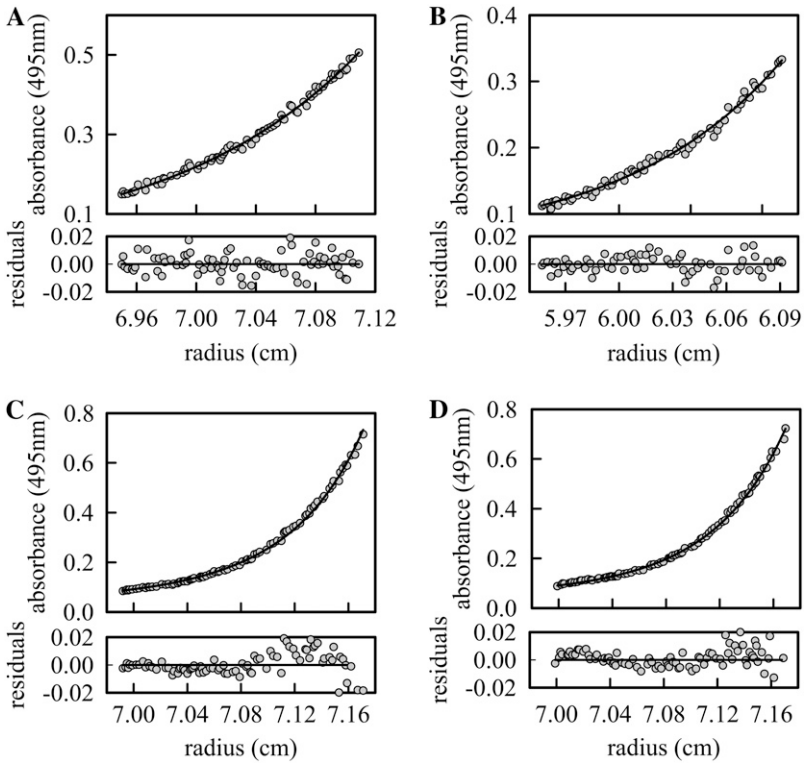

FIGURE 6 SE gradients recovered for samples containing CcpN repressor and the *gapB* and *pckA* target oligonucleotides. The gradients correspond to free *gapB*-Atto 647N (*A*), free *pckA*-Atto 647N (*B*), and CcpN complexes with *gapB*-Fl (*C*) and *pckA*-Fl (*D*). The concentration of free Atto 647N-labeled DNA was 1.5 μM. In the complexes, the concentration of DNA was 2.8 μM and the protein/DNA ratio was 7:1 in monomer units. Solid lines correspond to best fit of the data using one-component models for the free DNAs (*A* and *B*) and the two-species models discussed in the main text for the repressor/DNA mixtures (*C* and *D*).

achieved for a 1:3.2 mixture of free DNA and complex, in good agreement with the sedimentation coefficient distributions observed for this solution.

Analogously, the experimental CcpN/*gapB* gradients were compatible with a 3:1 mixture of complexes involving a CcpN dimer bound to 1 DNA molecule (bMw = 26,659) and a CcpN tetramer associated with two DNA units (bMw = 53,318). These complexes and their relative amounts agree well with those observed by SV analysis of the *gapB*/CcpN solutions. In summary, the stoichiometries recovered from the AUC experiments confirm those previously observed by FCCS-based titrations—4 CcpN monomers per DNA oligonucleotide for complexes involving the *pckA* target and 2 CcpN monomers for complexes involving the *gapB* target oligonucleotide—in excellent agreement with the results of the FCCS stoichiometry determinations.

Energetic analysis of CcpN titrations

Having established the stoichiometry of the complexes of the CcpN repressor with the target oligonucleotides, the FCCS binding isotherms shown in Fig. 3 were quantitatively analyzed in terms of free energies of formation of postulated complexes from the individual elements to assess the affinity and cooperativity of CcpN/operator interactions. In the case of the *gapB* target, two complexes, MO^B and M_2O^B, were postulated, where M represents monomeric CcpN and O^B is the *gapB* target oligonuleotide. Note that a simpler model, in which a single complex involving a repressor dimer bound to the target sequence, did not successfully describe the experimental data, consistent with the anisotropy results showing a monomer-dimer equilibrium over this concentration range. Comparison of the free energy changes associated with the binding of the first and second CcpN monomers to the *gapB* target (Table 3) reveals that the repressor binds cooperatively with the associated cooperativity higher than 1.7 kcal/mol.

In the case of the *pckA* target, the binding isotherm was fit using a model in which three complexes were postulated: MO^A, M_2O^A, and M_4O^A, where M is again a CcpN monomer and O^A is the *pckA* oligonucleotide. These species are all required, as we demonstrated that at 10 nM the protein is predominantly monomeric and that at the plateau the complex corresponds to 4 CcpN monomers on the *pckA* target. Interestingly, we find (Table 3) that the binding of a repressor monomer to the *pckA* target sequence is quite unfavorable and that the cooperativity associated with the binding of the dimer is comparable to that recovered for the *gapB* target (>1.6 kcal/

TABLE 3 Energetics of CcpN binding to the *gapB* and *pckA* oligonucleotides

	ΔG *pckA* (kcal/mol)	ΔG *gapB* (kcal/mol)
$M+O \leftrightarrow MO$	9.0 (<10.4)	8.6 (<9.4)
$2M+O \leftrightarrow M_2O$	19.6 (−0.5, +0.3)	18.9 ± 0.2
$M+MO \leftrightarrow M_2O$	>10.6	>10.3
$4M+O \leftrightarrow M_4O$	37.8 (−0.7, +0.6)	
$2M+M_2O \leftrightarrow M_4O$	18.2	

M and O represent a CcpN monomer and a molecule of the target oligonucleotide, respectively. ΔG values correspond to the dissociation reaction, and they are in kcal/mol. Errors were calculated by rigorous confidence limit testing at the 67% confidence level.

mol). The second dimer appears to bind with lower affinity than the first, but this may arise from the differences in the repeated recognition sequences forming the *pckA* target. Elucidation of the specificity determinants for the CcpN-DNA interactions will be the object of future studies.

DISCUSSION

This study demonstrates the usefulness of FCCS, combined with other biophysical approaches, for detailed characterization of protein-DNA interactions under true equilibrium conditions in solution. We investigated a newly identified transcriptional repressor, CcpN, which binds to two target operators, *gapB* and *pckA*. Although the interactions of the regulator with these two targets had been previously investigated by means of gel shift assays (25,28), the stoichiometry of the complexes remained to be determined. FCCS has the appropriate sensitivity to analyze these interactions, which occur in the nanomolar concentration range. Methods with comparable sensitivity, such as single-channel FCS and fluorescence anisotropy, were not applicable in this case because of the modest size changes associated with the formation of the complexes and/or the contribution from local rotational motions.

Hence, no shifts in the FCS profiles of the free DNA were observed upon saturation with CcpN repressor, and the anisotropy change associated with the binding of the protein to the labeled DNA was too small to allow precise evaluation of the interactions. Importantly, FCCS methods provided information concerning the stoichiometry of the CcpN-DNA complexes from the same data as those used for the determination of their affinity and cooperativity. This represents a major advantage over other methods commonly used to investigate protein-DNA interactions. For example, the long global tumbling times of the complexes (180 and 250 ns for the CcpN *gapB* and *pckA* complexes, respectively, estimated from low resolution models) compared with the lifetimes of the fluorophores commonly used to label biomolecules (~4 ns) precluded the use of time-resolved fluorescence anisotropy methods to determine the size and hence stoichiometry of the complexes.

The results of the FCCS experiments demonstrated directly and unambiguously that the stoichiometry of the complexes of CcpN with its two targets differed by a factor of two. Indeed no information about the self-association state of the protein was required to obtain this relative information, which can be quite useful in the evaluation of the influence of ligands, solution conditions (i.e., salt concentration), or DNA sequence on the stoichiometry of protein-DNA complexes. FCCS results also indicated that the absolute stoichiometries were 2:1 on the *gapB* target and 4:1 on the *pckA* target. We used alternate methods, in particular AUC, fluorescence anisotropy, and hydrodynamic modeling, to confirm the absolute stoichiometries suggested by the FCCS results. In general, if one has information concerning the self-association of the protein itself, then FCCS can be used alone to simultaneously determine the protein-DNA complex stoichiometry.

In principle, information concerning protein association states can also be obtained directly from fluctuation spectroscopy through concentration-dependent molecular brightness measurements of the protein alone. Such an approach was not used here due to our particularly low labeling ratio for the protein. However, we note that one of the most important applications of FCCS-based determinations of protein-DNA stoichiometries may well be in vivo experiments, and in these cases, the proteins are generally expressed as fusions with fluorescent proteins and hence are nearly 100% labeled. Moreover, all the complementary techniques used here are precluded in such in vivo studies. Simultaneous determination of stoichiometry by FCCS may also prove to be useful in vitro in cases where the ability to express and purify sufficient quantities of stable protein for AUC experiments is limiting. In these cases, if one can achieve nearly 100% labeling and limit the formation of aggregates, then the association properties of the protein alone can be determined.

Our experiments show that the structure of CcpN DNA complexes is strongly dependent on the target sequence involved. Thus, the *gapB* target oligonucleotide used here binds a dimer of the repressor, whereas four CcpN monomers are detected in the complexes with the *pckA* target. Moreover, the energetic analysis of the FCCS binding profiles reveals very cooperative binding of CcpN dimers to both operator DNAs. We also show that CcpN self-associates in a concentration-dependent manner (Kd 170 nM for the monomer-dimer equilibrium). Given that the specificity determinants recognized by CcpN are still not fully clarified (25,28), the biological implications of the distinct binding modes in terms of the in vivo regulation mechanisms of *gapB* and *pckA* genes by CcpN remain to be determined. In any case, the method described here, which allows the simultaneous estimation of stoichiometry, affinity, and cooperativity under equilibrium binding conditions should allow a thorough biological investigation of this and many other systems. Given the uncertainty concerning protein-DNA complex stoichiometry that often complicates the study of such systems, we anticipate that FCCS will find numerous applications in the field.

We thank Dr Acuña for helpful discussions and G. Bernabeu for technical assistance.

This work was supported by the European Community through the Marie Curie program (MERGT-CT-2006-046474), an instrumentation grant from the Association pour la Recherche contre le Cancer (grant No. 7882), funding from INSERM and the Agence National pour la Recherche to CAR, and a grant (BFU2006-03905/BMC) of the Spanish Dirección General de Enseñanza Superior e Investigación. S.Z. is the recipient of an I3P postdoctoral contract.

REFERENCES

1. Kim, S. A., K. G. Heinze, K. Bacia, M. N. Waxham, and P. Schwille. 2005. Two-photon cross-correlation analysis of intracellular reactions with variable stoichiometry. *Biophys. J.* 88:4319–4336.

2. Swift, J. L., R. Heuff, and D. T. Cramb. 2006. A two-photon excitation fluorescence cross-correlation assay for a model ligand-receptor binding system using quantum dots. *Biophys. J.* 90:1396–1410.

3. Hwang, L., and T. Wohland. 2004. Dual-color fluorescence cross-correlation spectroscopy using single laser wavelength excitation. *ChemPhysChem.* 5:549–551.

4. Rippe, K. 2000. Simultaneous binding of two DNA duplexes to the NtrC-enhancer complex studied by two-color fluorescence cross-correlation spectroscopy. *Biochemistry.* 39:2131–2139.

5. Strohner, R., M. Wachsmuth, K. Dachauer, J. Mazurkiewicz, J. Hochstatter, K. Rippe, and G. Langst. 2005. A 'loop recapture' mechanism for ACF-dependent nucleosome remodeling. *Nat. Struct. Mol. Biol.* 12:683–690.

6. Bacia, K., S. A. Kim, and P. Schwille. 2006. Fluorescence cross-correlation spectroscopy in living cells. *Nat. Methods.* 3:83–89.

7. Bacia, K., and P. Schwille. 2003. A dynamic view of cellular processes by in vivo fluorescence auto- and cross-correlation spectroscopy. *Methods.* 29:74–85.

8. Margeat, E., H. Boukari, and C. A. Royer. 2007. The characterization of biomolecular interactions using fluorescence fluctuation techniques. *In* P. Schuck, editor. Protein Interactions. Springer, New York. 1–38.

9. Schwille, P., F. J. Meyer-Almes, and R. Rigler. 1997. Dual-color fluorescence cross-correlation spectroscopy for multicomponent diffusional analysis in solution. *Biophys. J.* 72:1878–1886.

10. Bacia, K., I. V. Majoul, and P. Schwille. 2002. Probing the endocytic pathway in live cells using dual-color fluorescence cross-correlation analysis. *Biophys. J.* 83:1184–1193.

11. Liu, P., T. Sudhaharan, R. M. L. Koh, L. C. Hwang, S. Ahmed, I. N. Maruyama, and T. Wohland. 2007. Investigation of the dimerization of proteins from the epidermal growth factor receptor family by single wavelength fluorescence cross-correlation spectroscopy. *Biophys. J.* 93:684–698.

12. Rosales, T., V. Georget, D. Malide, A. Smirnov, J. Xu, C. Combs, J. R. Knutson, J. C. Nicolas, and C. A. Royer. 2007. Quantitative detection of the ligand-dependent interaction between the androgen receptor and the co-activator, Tif2, in live cells using two color, two photon fluorescence cross-correlation spectroscopy. *Eur. Biophys. J.* 36: 153–161.

13. Kim, S. A., K. G. Heinze, M. N. Waxhman, and P. Schwille. 2004. Intracellular calmodulin availability accessed with two-photon cross-correlation. *Proc. Natl. Acad. Sci. USA.* 101:105–110.

14. Heinze, K. G., A. Koltermann, and P. Schwille. 2000. Simultaneous two-photon excitation of distinct labels for dual-color fluorescence crosscorrelation analysis. *Proc. Natl. Acad. Sci. USA.* 97:10377–10382.

15. Schwille, P., U. Haupts, S. Maiti, and W. W. Webb. 1999. Molecular dynamics in living cells observed by fluorescence correlation spectroscopy with one- and two-photon excitation. *Biophys. J.* 77:2251–2265.

16. Larson, D. R., J. A. Gosse, D. A. Holowka, B. A. Baird, and W. W. Webb. 2005. Temporally resolved interactions between antigen-stimulated IgE receptors and Lyn kinase on living cells. *J. Cell Biol.* 171:527–536.

17. Muto, H., I. Nagao, T. Demura, H. Fukuda, M. Kinjo, and K. T. Yamamoto. 2006. Fluorescence cross-correlation analyses of the molecular interaction between an Aux/IAA protein, MSG2/IAA19, and protein-protein interaction domains of auxin response factors of Arabidopsis expressed in HeLa cells. *Plant Cell Physiol.* 47:1095–1101.

18. Weidemann, T., M. Wachsmuth, M. Tewes, K. Rippe, and J. Langowski. 2002. Analysis of ligand binding by two-colour fluorescence cross-correlation spectroscopy. *Single Molecules.* 3:49–61. Available at: http://www3.interscience.wiley.com/cgi-bin/fulltext/91015734/PDFSTART.

19. Swift, J. L., M. C. Burger, D. Massotte, T. E. S. Dahms, and D. T. Cramb. 2007. Two-photon excitation fluorescence cross-correlation assay for ligand-receptor binding: cell membrane nanopatches containing the human mu-opioid receptor. *Anal. Chem.* 79:6783–6791.

20. Merkle, D., W. D. Block, Y. P. Yu, S. P. Lees-Miller, and D. T. Cramb. 2006. Analysis of DNA-dependent protein kinase-mediated DNA end joining by two-photon fluorescence cross-correlation spectroscopy. *Biochemistry.* 45:4164–4172.

21. Collini, M., M. Caccia, G. Chirico, F. Barone, E. Dogliotti, and F. Mazzei. 2005. Two-photon fluorescence cross-correlation spectroscopy as a potential tool for high-throughput screening of DNA repair activity. *Nucleic Acids Res.* 33:e165.

22. Jahnz, M., and P. Schwille. 2005. An ultrasensitive site-specific DNA recombination assay based on dual-color fluorescence cross-correlation spectroscopy. *Nucleic Acids Res.* 33:e60.

23. Doi, N., H. Takashima, M. Kinjo, K. Sakata, Y. Kawahashi, Y. Oishi, R. Oyama, E. Miyamoto-Sato, T. Sawasaki, Y. Endo, and H. Yanagawa. 2002. Novel fluorescence labeling and high-throughput assay technologies for in vitro analysis of protein interactions. *Genome Res.* 12: 487–492.

24. Fillinger, S., S. Boschi-Muller, S. Azza, E. Dervyn, G. Branlant, and S. Aymerich. 2000. Two glyceraldehyde-3-phosphate dehydrogenases with opposite physiological roles in a nonphotosynthetic bacterium. *J. Biol. Chem.* 275:14031–14037.

25. Servant, P., D. Le Coq, and S. Aymerich. 2005. CcpN (YqzB), a novel regulator for CcpA-independent catabolite repression of *Bacillus subtilis* gluconeogenic genes. *Mol. Microbiol.* 55:1435–1451.

26. Licht, A., S. Preis, and S. Brantl. 2005. Implication of CcpN in the regulation of a novel untranslated RNA (SR1) in Bacillus subtilis. *Mol. Microbiol.* 58:189–206.

27. Fischer, E., and U. Sauer. 2005. Large-scale in vivo flux analysis shows rigidity and suboptimal performance of *Bacillus subtilis* metabolism. *Nat. Genet.* 37:636–640.

28. Licht, A., and S. Brantl. 2006. Transcriptional repressor CcpN from *Bacillus subtilis* compensates asymmetric contact distribution by cooperative binding. *J. Mol. Biol.* 364:434–448.

29. Zorrilla, S., T. Doan, C. Alfonso, E. Margeat, A. Ortega, G. Rivas, S. Aymerich, C. A. Royer, and N. Declerck. 2007. Inducer-modulated cooperative binding of the tetrameric CggR repressor to operator DNA. *Biophys. J.* 92:3215–3227.

30. Nagy, A., J. R. Wu, and K. M. Berland. 2005. Observation volumes and gamma-factors in two-photon fluorescence fluctuation spectroscopy. *Biophys. J.* 89:2077–2090.

31. Ha, T., I. Rasnik, W. Cheng, H. P. Babcock, G. H. Gauss, T. M. Lohman, and S. Chu. 2002. Initiation and re-initiation of DNA unwinding by the *Escherichia coli* Rep helicase. *Nature.* 419:638–641.

32. Blin, G., E. Margeat, K. Carvalho, C. A. Royer, C. Roy, and C. Picart. 2008. Quantitative analysis of the binding of ezrin to large unilamellar vesicles containing phosphatidylinositol 4,5 bisphosphate. *Biophys. J.* 94:1021–1033.

33. Royer, C. A., W. R. Smith, and J. M. Beechem. 1990. Analysis of binding in macromolecular complexes: a generalized numerical approach. *Anal. Biochem.* 191:287–294.

34. Chatelier, R. C. 1988. A parameterized overspeeding method for the rapid attainment of low-speed sedimentation equilibrium. *Anal. Biochem.* 175:114–119.

35. Schuck, P. 2000. Size-distribution analysis of macromolecules by sedimentation velocity ultracentrifugation and Lamm equation modeling. *Biophys. J.* 78:1606–1619.

36. Laue, T. M., B. D. Shah, T. M. Ridgeway, and S. L. Pelletier. 1992. Computer-aided interpretation of analytical sedimentation data for proteins. *In* Analytical Ultracentrifugation in Biochemistry and Polymer Science. S. E. Harding and A. J. Rowe, editors. Cambridge, UK, The Royal Society of Chemistry. 90–125.

37. Minton, A. P. 1994. Conservation of signal: a new algorithm for the elimination of the reference concentration as an independently variable parameter in the analysis of sedimentation equilibrium. *In* Modern Analytical Ultracentrifugation: Acquisition and Interpretation of Data for Biological and Synthetic Polymer Systems. T. M. Schuster and T. M. Laue, editors. Birkhauser, Boston, MA. 81–93.

38. Rivas, G., W. Stafford, and A. P. Minton. 1999. Characterization of heterologous protein-protein interactions using analytical ultracentrifugation. *Methods*. 19:194–212.

39. Garcia De La Torre, J., M. L. Huertas, and B. Carrasco. 2000. Calculation of hydrodynamic properties of globular proteins from their atomic-level structure. *Biophys. J*. 78:719–730.

40. Ortega, A., and J. G. de la Torre. 2007. Equivalent radii and ratios of radii from solution properties as indicators of macromolecular conformation, shape, and flexibility. *Biomacromolecules*. 8:2464–2475.

41. Garcia de la Torre, J., and B. Carrasco. 2002. Hydrodynamic properties of rigid macromolecules composed of ellipsoidal and cylindrical subunits. *Biopolymers*. 63:163–167.

42. Valeur, B. 2002. Molecular Fluorescence: Principles and Applications. Wiley-VCH, Weinheim, Germany.

43. Bayley, P., S. Martin, P. Browne, and C. Royer. 2003. Time-resolved fluorescence anisotropy studies show domain-specific interactions of calmodulin with IQ target sequences of myosin V. *Eur. Biophys. J*. 32: 122–127.